Atmos. Chem. Phys., 15, 11461–11476, 2015
www.atmos-chem-phys.net/15/11461/2015/
doi:10.5194/acp-15-11461-2015

Atmospheric Chemistry and Physics
Open Access

The impacts of volcanic aerosol on stratospheric ozone and the Northern Hemisphere polar vortex: separating radiative-dynamical changes from direct effects due to enhanced aerosol heterogeneous chemistry

S. Muthers[1,2], F. Arfeuille[3], C. C. Raible[1,2], and E. Rozanov[4,5]

[1]Climate and Environmental Physics, University of Bern, Bern, Switzerland
[2]Oeschger Centre for Climate Change Research, University of Bern, Bern, Switzerland
[3]Suisse Federal Laboratories for Material Science and Technology (Empa) Duebendorf, Switzerland
[4]Institute for Atmospheric and Climate Science, ETH, Zurich, Switzerland
[5]Physikalisch-Meteorologisches Observatorium Davos and World Radiation Center (PMOD/WRC), Davos, Switzerland

Correspondence to: S. Muthers (muthers@climate.unibe.ch)

Received: 30 March 2015 – Published in Atmos. Chem. Phys. Discuss.: 20 May 2015
Revised: 30 August 2015 – Accepted: 10 September 2015 – Published: 16 October 2015

Abstract. After major volcanic eruptions the enhanced aerosol causes ozone changes due to greater heterogeneous chemistry on the particle surfaces (HET-AER) and from dynamical effects related to the radiative heating of the lower stratosphere (RAD-DYN). We carry out a series of experiments with an atmosphere–ocean–chemistry–climate model to assess how these two processes change stratospheric ozone and Northern Hemispheric (NH) polar vortex dynamics. Ensemble simulations are performed under present day and preindustrial conditions, and with aerosol forcings representative of different eruption strength, to investigate changes in the response behaviour. We show that the halogen component of the HET-AER effect dominates under present-day conditions with a global reduction of ozone (−21 DU for the strongest eruption) particularly at high latitudes, whereas the HET-AER effect increases stratospheric ozone due to N_2O_5 hydrolysis in a preindustrial atmosphere (maximum anomalies +4 DU). The halogen-induced ozone changes in the present-day atmosphere offset part of the strengthening of the NH polar vortex during mid-winter (reduction of up to $-16\,m\,s^{-1}$ in January) and slightly amplify the dynamical changes in the polar stratosphere in late winter ($+11\,m\,s^{-1}$ in March). The RAD-DYN mechanism leads to positive column ozone anomalies which are reduced in a present-day atmosphere by amplified polar ozone depletion (maximum anomalies +12 and +18 DU for present day and preindustrial, respectively). For preindustrial conditions, the ozone response is consequently dominated by RAD-DYN processes, while under present-day conditions, HET-AER effects dominate. The dynamical response of the stratosphere is dominated by the RAD-DYN mechanism showing an intensification of the NH polar vortex in winter (up to $+10\,m\,s^{-1}$ in January). Ozone changes due to the RAD-DYN mechanism slightly reduce the response of the polar vortex after the eruption under present-day conditions.

1 Introduction

Tropical eruptions strong enough to inject into the stratosphere perturb the physical and the chemical states of the climate system for several years and longer (Robock, 2000; Cole-Dai, 2010; Timmreck, 2012). Although a range of gases are injected (e.g. Textor et al., 2004), the global climate impacts stem from the aerosol produced from the injected sulfur dioxide (SO_2). In the stratosphere volcanically injected SO_2 is converted into sulfuric acid ($H_2SO_4 + H_2O$) aerosols that (i) reflect in the visible part of the solar spectrum, (ii) absorb terrestrial and solar infrared radiation, and (iii) provide surface for a large number of chemical reactions that alter the chemical composition of the stratosphere (Forster et al.,

Published by Copernicus Publications on behalf of the European Geosciences Union.

2007). The enhanced stratospheric aerosol increases the optical depth of the atmosphere, leading to a decrease in SW radiation in the troposphere and at the surface. Increased absorption of long wave and solar near-infrared radiation increases heating rates in the volcanic plume causing a pronounced warming of the tropical stratosphere. The perturbed vertical and meridional temperature gradients alter the stratospheric circulation and via interaction between the stratosphere and the troposphere affect surface climate. A prominent example for this mechanism is the winter warming pattern in the NH observed after several large tropical volcanic eruptions (Robock and Mao, 1992; Stenchikov et al., 2002; Shindell et al., 2004; Fischer et al., 2007; Christiansen, 2008; Zanchettin et al., 2012). Such surface temperature anomalies over Eurasia are related to a positive phase of the Arctic Oscillation, which is forced by interactions between the stratospheric polar vortex and tropospheric circulation patterns (Graf et al., 1993; Kodera, 1994).

The overall impact of a tropical eruption on stratospheric ozone chemistry can be separated into the effect from (i) altered reaction rates due to change in temperature, (ii) enhanced heterogeneous chemistry from elevated sulfuric acid aerosol surface area density (SAD), (iii) the temperature and aerosol changes in modifying the occurrence and types of polar stratospheric clouds (PSCs), (iv) the composition changes induced by the dynamical perturbations in the stratosphere, and (v) changes in photolysis rates from the enhanced aerosol. The temperature change and the reactions on the heterogeneous aerosol surfaces mainly take place in the aerosol cloud. The heterogeneous conversion of nitrogen oxides (N_2O_5) into nitric acid (HNO_3) slows down the NO_x cycle of catalytic ozone destruction, with the effect of increasing ozone concentrations in the middle stratosphere (Tie and Brasseur, 1995; Solomon et al., 1996). In the lower stratosphere, the Cl_x and HO_x cycles are more important with the net chemical effect being ozone loss in the present-day atmosphere (Tie and Brasseur, 1995; Solomon et al., 1996; SPARC, 2013). The chemical ozone loss from an eruption in the present-day atmosphere is intensified at high latitudes by a strengthening of the polar vortex, which reduces temperatures, increasing PSC occurrence. Additionally, the presence of H_2SO_4 in the polar stratosphere in combination with colder temperatures facilitates the formation of liquid sulfuric acid ternary solution particles, which further increase SAD and therefore ozone loss (Carslaw et al., 1994).

The net effect of the chemical response further depends on the background composition of the atmosphere. The slowdown of the NO_x cycle and heterogeneous reactions intensify the chlorine cycle of ozone destruction, but chlorine levels have undergone serious changes in the last decades (Solomon, 1999). In the present-day atmosphere, the elevated halogen loading in the stratosphere means that the net chemical effect of the eruption on the global ozone abundance is a reduction (Tie and Brasseur, 1995; Rozanov et al., 2002; Austin et al., 2013). For low halogen loadings, however, the chemical effect of the eruption is to increase ozone globally (Tie and Brasseur, 1995; Anet et al., 2013; Austin et al., 2013). Furthermore, increase in the stratospheric water vapour concentrations associated with the warming of the tropical tropopause can accelerate the HO_x cycle and reduce ozone even in the case of low halogen concentrations (Heckendorn et al., 2009).

These effects on stratospheric ozone can broadly be classified into two distinct groups. The first involves composition-dynamical interactions associated with the radiative absorption of the volcanic aerosol, which we refer to as RAD-DYN. The second comprises the net change due to a large number of heterogeneous chemical reactions on the aerosol surface, which we refer to as HET-AER. Please note, that the RAD-DYN effect includes also chemical effects, for instance though changes in the reactions rates or PSC formation due to the temperature changes. Moreover, HET-AER processes affect also the radiation transfer through the atmosphere by changes in the chemical composition.

From the observations it is not possible to understand which processes are responsible for the ozone changes and how these changes affect the dynamics. Using model simulations, the attribution of the ozone changes after the Mt. Pinatubo eruption has been assessed in several studies (Brasseur and Granier, 1992; Pitari and Rizi, 1993; Al-Saadi et al., 2001; Telford et al., 2009; Aquila et al., 2013). In general, these studies conclude that both mechanisms are important, with regional and seasonal differences.

In the tropics, total column ozone was observed to reduced after the eruption of Mt. Pinatubo (Randel and Wu, 1995) which was a combined signal of a reduction in the lower stratosphere and an increase of ozone concentrations above (Grant et al., 1994). The reduction in the lower stratosphere has been attributed to a mix of the dynamic effect and heterogeneous chemical reactions (Rosenfield et al., 1997; Rozanov et al., 2002). The former reduces ozone by enhanced up-welling of ozone poor air and the latter via chemical depletion by active chlorine. Above 18 hPa the NO_x deactivation dominates, increasing ozone with further enhancement in the tropics due to modified photolysis (Pitari and Rizi, 1993). A negative feedback between the tropical ozone changes and aerosol heating has been suggested by Al-Saadi et al. (2001), with an reduced heating of up to 25 % in the tropical middle stratosphere.

Ozone changes in the NH are thought to be primarily caused by the heterogeneous chemical reaction effects (Pitari and Rizi, 1993; Aquila et al., 2013), in particular at high latitudes (Portmann et al., 1996; Solomon et al., 1996; Rosenfield et al., 1997; Telford et al., 2009; Pitari et al., 2014). By contrast, the increasing ozone observed in the Southern Hemisphere (SH) has been attributed to dynamical processes induced by the aerosol heating in combination with the phase of the Brewer–Dobson circulation (Aquila et al., 2013; Dhomse et al., 2014) or the Quasi-Biennial Oscillation (QBO) (Telford et al., 2009; Randel and Wu, 1995).

The stratospheric dynamic perturbation after volcanic eruptions originates mainly from the aerosol heating in the tropical lower stratosphere. Nevertheless, changes in the ozone concentrations also affect heating rates and therefore modulate the dynamic response to the eruption (Muthers et al., 2014a). Using observed ozone anomalies for the Mt. Pinatubo eruption, Stenchikov et al. (2002) found a strengthening of the Arctic Oscillation (AO) in late winter and early spring after the eruption, which is explained by the cooling effect of the polar stratospheric ozone depletion. However, by forcing the model with observed ozone anomalies, a separation of the dynamical and chemical causes of the ozone changes is not possible. Similar results were found by Shindell et al. (2003) who compared the Mt. Pinatubo eruption in simulations with and without ozone changes. For a different climate state (Mt. Tambora, 1815) without anthropogenic chlorine in the stratosphere, they found a very small influence of the ozone changes on the dynamical perturbation.

The purpose of this study is to deepen our understanding of the processes which drive ozone changes after a strong tropical volcanic eruption and how these changes modulate atmospheric dynamics in the stratosphere. Moreover, we assess the influence of the eruption strength on these changes and the role of different climate setting in moderating the dynamical responses, where the term climate setting describes a specific atmospheric composition of greenhouse gases and their effects on the climate system. To the best of our knowledge these questions have not been addressed before. Here, we use a set of ensemble sensitivity simulations performed by the atmosphere–ocean–chemistry–circulation model (AOCCM) SOCOL-MPIOM. To evaluate the dynamic response, this study focuses mainly on the NH and on the winter season.

The paper is structured as follows: Sect. 2 introduces the coupled AOCCM, the forcing data, and the setup of the experiments. The results are presented in Sect. 3, first for the simulated ozone changes associated with the different processes (Sect. 3.1), followed by the dynamical changes (Sect. 3.2). Section 3.3 focuses on interactions between the ozone chemistry and the dynamic response associated with the RAD-DYN effects. Finally, we discuss the results and present conclusive remarks in Sect. 4.

2 Model and experiments

2.1 SOCOL-MPIOM

SOCOL-MPIOM is a coupled atmosphere–ocean–chemistry–climate model (Muthers et al., 2014b). The atmospheric-chemistry component SOCOL version 3 (Schraner et al., 2008; Stenke et al., 2013) is based on the physical component MA-ECHAM5 (Roeckner et al., 2003; Manzini et al., 2006), which is coupled to the chemistry module MEZON (Rozanov et al., 1999; Egorova et al., 2003). The chemistry module uses temperature fields from ECHAM5 and calculates the tendency of 41 gas species, taking into account 200 gas-phase, 16 heterogeneous, and 35 photolytical reactions. Heterogeneous reactions are parametrised following Carslaw et al. (1995) and can take place in/on aqueous sulfuric acid aerosols and on three types of polar stratospheric clouds.

In the short-wave scheme of SOCOL the solar spectrum is divided into six spectral intervals. The scheme considers Rayleigh scattering, scattering on aerosols and clouds, and the absorption of solar irradiance in UV-induced photolysis reactions, by O_3, O_2, and 44 other species. In the near-infrared intervals absorption by water vapour, CO_2, N_2O, CH_4, and O_3 is implemented. Furthermore, a parametrisation for the absorption of radiation by O_2 and O_3 in the Lyman-alpha, Schumann–Runge, Hartley and Higgins bands is implemented following an approach similar to Egorova et al. (2004). The long-wave scheme considers frequencies from 10 to 3000 cm^{-1} for the absorption by water vapour, CO_2, O_3, N_2O, CH_4, CFC-11, CFC-12, CFC-22, aerosols, and clouds. Chemistry–climate interactions can optionally be disabled in the model, by deactivating the interactive chemistry module. In this case, 3-D time-dependent ozone data needs to be applied as forcing.

The spectral truncation used in this study is T31, which corresponds to a horizontal resolution of approximately $3.75^\circ \times 3.75^\circ$. In the vertical, the atmosphere is divided into 39 levels with the highest level at 0.01 hPa (80 km). With this vertical resolution the model is not able to produce a QBO by itself; therefore a QBO nudging is applied (Giorgetta et al., 1999).

The atmosphere–chemistry model SOCOL is coupled to the ocean model MPIOM which includes a sea ice module (Marsland, 2003; Jungclaus et al., 2006). MPIOM is used in a nominal resolution of 3°, with the poles shifted to Greenland and Antarctica to avoid numerical singularities at the poles. This setup allows for a high resolution in the deep water formation region of the North Atlantic. Both models, MPIOM and SOCOL are coupled by the OASIS3 coupler (Budich et al., 2010; Valcke, 2013).

2.2 Aerosol forcing data sets

To simulate the climatic effect of a volcanic eruption in SOCOL-MPIOM, the model needs information about the optical properties of the aerosols, including extinction coefficients, single scattering albedo, and the asymmetry factor for each spectral interval, latitude, vertical level, and time step. Furthermore, the chemistry module needs the surface area density (SAD) of the aerosols. In a sensitivity study for different eruption sizes, these forcings need to be generated in a consistent manner, to allow for a fair comparison between the eruptions.

Since nucleation, condensation, coagulation, and sedimentation of the aerosols change in different ways with the SO_2

concentration (Timmreck et al., 2010), a simple linear scaling of observation-based aerosol data sets by the sulfur mass may lead to an unrealistic forcing data set. The aerosol coagulation process, for instance, depends on the SO_2 concentration, and hence particles tend to be larger as we inject more SO_2. The increase in total SAD is hence not proportional to the increase in SO_2 mass. Conversely, the total stratospheric warming depends on the aerosol absorption in the infrared and varies more or less linearly with the SO_2 mass injected (Grainger et al., 1995). However, an increase in the sedimentation rates with larger aerosols further modifies the relationship between the stratospheric warming and the initial sulfur mass released.

The aerosol data set used here was therefore calculated offline using the micro-physical aerosol model AER (Weisenstein et al., 1997, 2007). AER is a 2-D model with global domain, resolving the atmosphere from the surface to approximately 60 km altitude. The vertical resolution is about 1.2 km with a horizontal grid spacing of 9.5° of latitude. To simulate the formation of the aerosols, the SO_2 injection mass, as well as the timing and latitude/altitude of the injection are used as inputs for the AER model. Three AER simulations were carried out with 15, 30, and 60 Tg of SO_2 injected, the former corresponding approximately to the SO_2 detected in the stratosphere shortly after the Pinatubo eruption (Guo et al., 2004). Furthermore, the timing (middle of June) and the location (5° S–14° N between 23 and 25 km) are chosen to fit the Pinatubo 1991 eruption. Besides the sulfur mass, the same set of initial and boundary conditions were applied in all three simulations, corresponding to the atmospheric state at the time of the eruption of Mt. Pinatubo in 1991 (Fleming et al., 1999).

SAD values and extinction coefficients in the visible are shown in Fig. 1 for the DJF (December–January–February) season in the first winter after the eruption on the left and as Hovmoeller diagram for SAD and extinctions at 50 hPa on the right. Arfeuille et al. (2013) found that an injection of 14 Tg of SO_2 (7 Tg of sulfur) produced mid-visible extinctions much higher than observed in the tropical stratosphere after the Pinatubo eruption. As shown by Dhomse et al. (2014), the peak burden of sulfur in the particle phase was around a factor of 2 lower than the peak sulfur burden in the gas phase, in the range 3.7–6.7 Tg of sulfur. The 15 Tg AER simulation shall therefore be regarded as an upper limit for the perturbation that occurred following Pinatubo. Furthermore, some differences in the shape of the AER aerosol forcing and observations for Pinatubo exists. Using satellite based aerosol forcings, the agreement with observations can be improved for Pinatubo (Arfeuille et al., 2013). However, due to the non-linear relationship between sulfur mass and the aerosol properties satellite based aerosol records can not be applied in this sensitivity study. A detailed comparison of satellite based aerosol data sets and the AER method is given in Arfeuille et al. (2013).

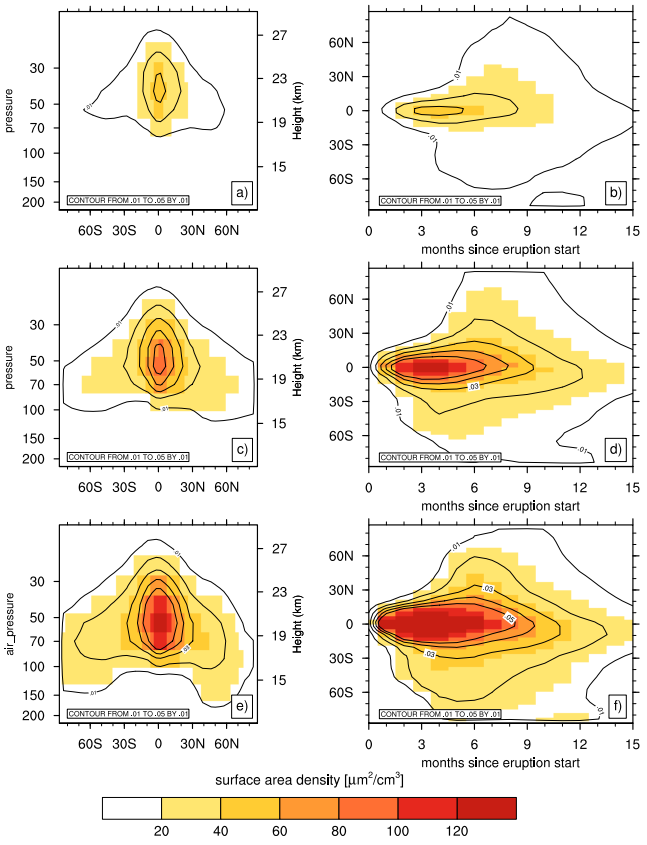

Figure 1. Aerosol data sets used in the simulations for the 15 Tg **(a, b)**, 30 Tg **(c, d)**, and 60 Tg **(e, f)** SO_2 aerosol forcing. Surface area densities (SADs) are displayed by colours; contours denote extinction rates in the visible (440–690 nm) with contours from 0 to 0.05 by an interval of 0.01 km^{-1}. The column on the left displays averages for the first post-eruption winter season (DJF) as a function of pressure and latitude, while the right column shows Hovmöller diagrams of the monthly mean SAD forcing at 50 hPa.

2.3 Experiments

A number of ensemble sensitivity experiments were performed. The experiments differ in the aerosol forcing, the atmospheric composition of different ozone depleting substances (ODSs) and other greenhouse gases (GHGs), as well as the physical and chemical processes considered.

To assess the role of the climate setting on the response, the eruptions either take place under present-day (early 1990s with high loads of ODS and GHG in the atmosphere) or preindustrial conditions (early 19th century, low concentrations of ozone depleting halogens and GHG). The simulations therefore differ in their atmospheric composition, but also the climate state is different due to the effect of the GHG on temperature and dynamics. The initial states for the two periods are based on two transient simulations described in Muthers et al. (2014b). For the preindustrial climate simulations the restart files were selected between the years 1812

Table 1. Overview of the ensemble experiments used in this study. SO_2 mass refers to the aerosol amount assumed in the generation of the volcanic forcing (compare Sect. 2.2). Climate setting – PD: 1990s conditions with high concentrations of ozone depleting substances (ODS). PI: preindustrial atmosphere with low concentrations of ODS. Volcanic forcing – SAD: surface area density of the aerosols. OP: optical properties, i.e. extinction rates for all spectral intervals. For each ensemble, eight simulations are performed.

Ensemble	SO_2 mass (Tg)	Climate setting	Volcanic forcing	Atm. chemistry
PD[15,30,60]	15, 30, 60	PD	SAD and OP	interactive
PI[15,30,60]	15, 30, 60	PI	SAD and OP	interactive
PD[15,30,60]_HET-AER	15, 30, 60	PD	SAD	interactive
PI[15,30,60]_HET-AER	15, 30, 60	PI	SAD	interactive
PD[15,30,60]_RAD-DYN	15, 30, 60	PD	OP	interactive
PI[15,30,60]_RAD-DYN	15, 30, 60	PI	OP	interactive
PD[15,60]_o3	15, 60	PD	–	ozone from PD[15, 60]
PI[15,60]_o3	15, 60	PI	–	ozone from PI[15, 60]
PD[15,60]RAD-DYN_o3	15, 60	PD	–	ozone from PD[15, 60]_RAD-DYN
PI[15,60]RAD-DYN_o3	15, 60	PI	–	ozone from PI[15, 60]_RAD-DYN
PD_CTRL	–	PD	–	interactive
PI_CTRL	–	PI	–	interactive

and 1814. Present-day initial conditions were extracted between 1988 and 1990. Each ensemble consists of 8 simulations and the restart files were carefully selected to cover a wide range of different phases of the Atlantic Meridional Overturning Circulation and the tropical Pacific (ENSO). The timing of the eruption (middle of June) is identical for both climate settings.

For comparison, the simulated response of the climate system after the volcanic eruption is evaluated against an ensemble of control simulations for each climate setting. These simulations were initialised using the same set of initial conditions, but were forced by an aerosol data set representing the unperturbed background state of the atmosphere.

To distinguish between the aerosol forcings and the climate setting the simulations are named PI15, PI30, and PI60 for the eruption sizes of 15, 30, and 60 Tg of SO_2 in the preindustrial conditions, respectively. The present-day simulations are named PD15, PD30, and PD60, accordingly. These simulations consider the both radiative and the chemical aspects of the volcanic forcing (named full aerosol effect in the following) based on SAD values and optical properties generated by the AER model. Note that in this study we do not include the effects of the enhanced aerosol in reducing photolysis, and related composition changes. As explained in Sect. 2.2, the PD15 ensemble simulation represents an upper limit for the effects from the Mt. Pinatubo eruption in 1991. The PI60 ensemble is comparable to the Tambora eruption in 1815 (Gao et al., 2008) although the date of the eruption and the shape of the aerosol forcings is different (Arfeuille et al., 2014). All aerosol forcing time series were applied as zonal monthly means between 690 and 3.8 hPa and interpolated to the model levels in SOCOL-MPIOM.

Furthermore, the effect of stratospheric aerosols on the atmosphere is separated into radiative-dynamical perturbations (RAD-DYN) and changes related to heterogeneous chemical reactions on aerosol surfaces (HET-AER). In the RAD-DYN experiment, only the optical properties of the aerosols was applied as forcing and the pre-eruption values were used for the SAD. The HET-AER experiment was forced only with time-varying SAD with the optical properties representing pre-eruptive conditions. Ensemble experiments with 8 members (Table 1) for both processes were performed for the three eruption sizes of 15, 30, and 60 Tg of SO_2. In the following these experiments are identified by the suffix _HET-AER and _RAD-DYN. A summary of the experiments used in this study is given in Table 1.

Finally, we extract the simulated ozone changes for the full forcing and RAD-DYN experiments and apply them as forcing in an additional set of ensemble simulations. A configuration of SOCOL-MPIOM without interactive chemistry is used in these experiments (Muthers et al., 2014b). Since ozone concentrations are not allowed to change, these simulations isolate only the effect of the ozone changes on the dynamical perturbation. Consequently, aerosol forcings represent pre-eruptive conditions. Ozone concentrations are applied as daily mean values on the model grid, to avoid errors due to the vertical interpolation between pressure levels and model level. These experiments were performed for the 15 and 60 Tg aerosol forcing only.

The analysis presented mainly focuses on the first winter (DJF) after the eruption. Results are always expressed in terms of anomalies to the average of the control ensemble simulations for each climate setting. Significance estimates are based on a two-tailed Student's t test using the 5 % significance level.

3 Results

3.1 Ozone changes

3.1.1 Present-day conditions

The response of the global averaged column ozone (Fig. 2) reveals clear differences between the RAD-DYN and the HET-AER effect. In a present-day setup (Fig. 2 top) heterogeneous chemical reactions on the aerosol surface cause a depletion of global column ozone, which is significant for more than 2 years. Ozone is continuously reduced for about 9 months after the eruption, independent from the eruption size. However, the amplitude of the anomaly increases with the eruption size to −13, −18, and −21 DU. The recovery phase lasts about 24 months in all simulations, again independent of the eruption size. As expected, the spatial analysis of the HET-AER anomalies shows largest ozone depletion in the high latitudes of both hemispheres (Fig. 3a), in particular during spring and the polar ozone depletion through HET-AER processes increases with the eruption size (Fig. S1a, d, g in the Supplement).

Zonally averaged height profiles for the first winter after the eruption reveal that the aerosol heterogeneous chemical effect also leads to positive anomalies in the upper stratosphere above 30 hPa (Fig. 4a). However, these anomalies are present only in the first winter after the eruption and are to some extent compensated by negative anomalies in the lower stratosphere. The positive anomalies in the upper stratosphere are related to the slow-down of the NO_x cycle of catalytic ozone destruction, as N_2O_5 is converted into HNO_3 on the H_2SO_4 aerosols. By reducing the NO_x concentrations the reaction also slows down the deactivation of chlorine, which dominates ozone destruction in the lower atmosphere and explains the negative anomalies below 30 hPa. Furthermore, the conversion stops, when all N_2O_5 is consumed (Tie and Brasseur, 1995). In the lower stratosphere N_2O_5 is quickly consumed in the months after the eruption, first in the tropical latitudes, but about 5 months after the eruptions N_2O_5 is reduced by more than 80 % at all latitudes below around 30 hPa (not shown). In the NH and SH polar stratosphere in late winter and spring the heterogeneous reactions on the aerosol surfaces and on PSCs strongly increase the chlorine concentrations in the lower stratosphere and explain the pronounced reductions in ozone.

The RAD-DYN effect causes positive global mean column ozone anomalies after the eruption, which peak about 7 months after the beginning of the eruption (+5, +8, and +12 DU), and return to background conditions after about 18 months (Fig. 2). Similar to the chemical effects, no clear differences in terms of the duration are found between the three eruption sizes. The column ozone anomaly time series furthermore reveal some fluctuations, mainly during the first year. In February–March and July–August, the positive column ozone anomalies undergo clear reductions. These

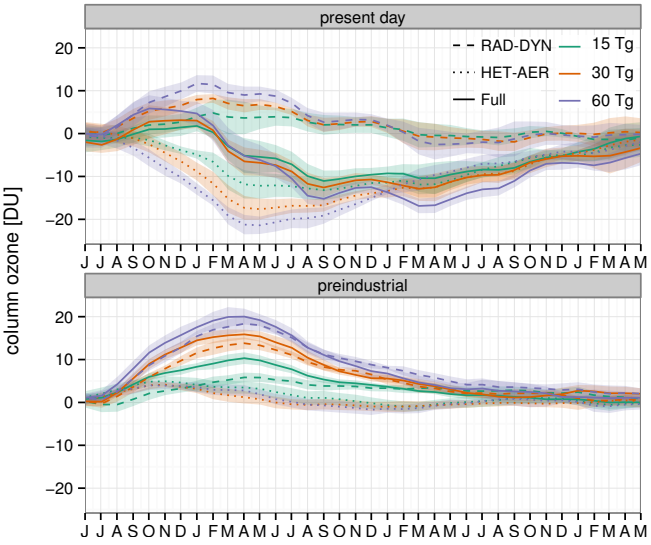

Figure 2. Monthly mean global mean anomalies of column ozone (DU) for present-day (top) and preindustrial conditions (bottom) for the ensemble simulations with the full forcing effect (full, solid lines), the ensemble simulations considering only the heterogeneous aerosol chemical effect of the aerosols (HET-AER, dotted lines), and the simulations forced only by the radiative-dynamical aerosol effects (RAD-DYN, dashed lines). The different eruption sizes are indicated by colours. Lines denote the ensemble mean, shading the standard deviation of the ensemble.

variations are related to the present-day polar ozone depletion in the NH and SH, which is further intensified after the eruption by colder conditions inside the polar vortices and chlorine activation on the PSCs (Fig. 3b). However, the polar ozone depletion in the RAD-DYN experiment is much weaker than the signal found in the HET-AER ensemble experiment. For the 15 Tg aerosol forcing the polar ozone depletion is rather moderate (Fig. 3b), but the polar ozone depletion intensifies and lasts longer with increasing forcing strength (Fig. S1e, h).

Overall, the spatial pattern of ozone anomalies due to the RAD-DYN effect is more heterogeneous than for the HET-AER effect (Fig. 3b). Reduced ozone column abundances are found at tropical latitudes and increasing concentrations at mid- to high-latitudes. The tropical reduction is related to pronounced ozone depletion at 30 hPa, which is partly compensated by positive ozone anomalies above and below (Fig. 4b). This equatorial anomaly pattern is very similar for all post-eruption seasons and remains significant until the end of the first year after the eruption (Fig. 3b). The circulation changes in the stratosphere that are responsible for the ozone anomalies are detected in the residual mean circulation anomaly (Andrews et al., 1987). The enhanced vertical transport of ozone changes the vertical ozone profile and replaces ozone-enhanced air at 30 hPa by ozone depleted air from lower levels. Air with enriched ozone from 30 hPa further increases ozone concentrations at 10 hPa and above. The

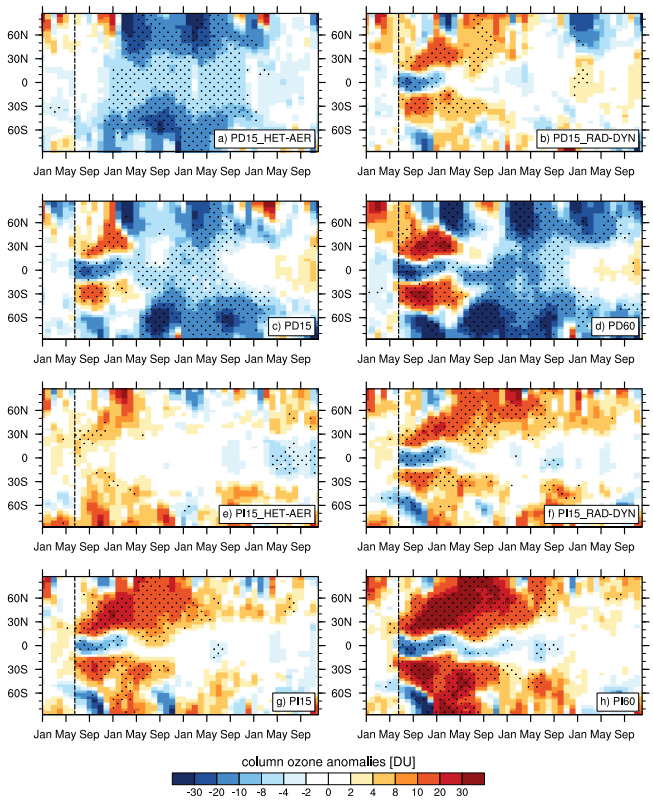

Figure 3. Zonal average monthly mean anomalies of total column ozone in different ensemble simulations: **(a)** anomalies due to the effect of heterogeneous chemical reactions for the 15 Tg eruption for present-day conditions. **(b)** Same as **(a)**, but for the radiative-dynamical effects of the aerosols. **(c)** Same as **(a)**, but for the full forcing simulations. **(d)** Full forcing simulations for the 60 Tg aerosol forcing data set. **(e–h)** Similar to **(a–d)**, but for preindustrial conditions. Stippling in the simulation panels indicates significant differences to the control (Student's t test $p \leq 0.05$). The beginning of the eruption is depicted by the vertical dashed line.

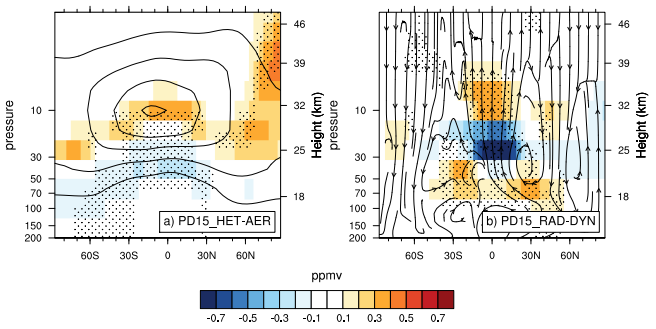

Figure 4. Ensemble mean zonal mean ozone mixing ratio anomalies (ppmv) for the first post eruption DJF season in the present-day ensemble experiment considering **(a)** the effect of aerosol heterogeneous chemical reactions **(b)** the radiative-dynamic effect with the 15 Tg aerosol forcing under present-day conditions. Contour lines in **(a)** denote the climatological average DJF ozone mixing ratios in the present-day control ensemble. The streamlines in **(b)** show the residual circulation anomalies (Andrews et al., 1987). Stippling indicates significant anomalies (Student's t test $p \leq 0.05$).

upward motion in the tropics is balanced by descending air masses in the mid-latitudes. Since these air masses originate from tropical latitudes, they transport ozone enriched air into the lower stratosphere of the mid-latitudes and create positive ozone anomalies. This meridional transport is visible in the positive anomalies of column ozone, which first occur in subtropical latitudes and reach the high latitudes several months later (Fig. 3b). A fraction of descending ozone is recirculated into the lowermost tropical stratosphere and leads to positive ozone anomalies at 70 hPa. Furthermore, changes in the incoming UV radiation and photodissociation by the high optical depth of the aerosols may affect ozone production in the tropics (Pitari and Rizi, 1993), but this process is not yet implemented in the model.

The full aerosol effect displays the combined influence of both processes (Fig. 2). In the first 7 months after the eruption, radiative-dynamical effects dominate the response of ozone with positive ozone anomalies, which reach maximum values of +2, +3, and +6 DU between autumn and early winter depending on the 15, 30, and 60 Tg forcing, respectively (Fig. 2). In the following months, the influence of the radiative-dynamical effects weakens, while chemical effects are still present and column ozone anomalies become negative for about 2 years. The imprint of the intensified polar ozone depletion is clearly visible in the full forcing experiment. With increasing eruption size the amplitude of the negative and positive anomalies increases, while the spatial patterns remain similar (Fig. 3d and S1f, i). The dynamical perturbation of the residual circulation by the RAD-DYN effects is also clearly visible in the full forcing experiments (Fig. S3a, b, c).

3.1.2 Preindustrial conditions

Changing the climatic background conditions from present-day to preindustrial has a strong impact on the HET-AER effect (Fig. 2 bottom and Fig. 3e). Without pronounced amounts of ODS in the stratosphere, the effect of heterogeneous chemical reactions on the chlorine cycle of ozone depletion is weak. Instead, the slow-down of the NO_x cycle of ozone depletion becomes important, explaining slight positive anomalies of column ozone, for a few months after the eruption. However, with maximum anomalies between +4 and +5 DU the response is not very pronounced. The size of the eruption has no significant effect on the ozone anomalies due to HET-AER effects (Fig. 2 bottom and S2d, g).

RAD-DYN effects introduce again positive anomalies of column ozone after the eruption (Figs. 2, 3f). In comparison to the present-day ensemble simulations, the anomalies are stronger (+6, +14, +18 DU), longer lasting and the variability is lower, which is explained by the reduced polar ozone depletion in a preindustrial atmosphere. In fact, the positive

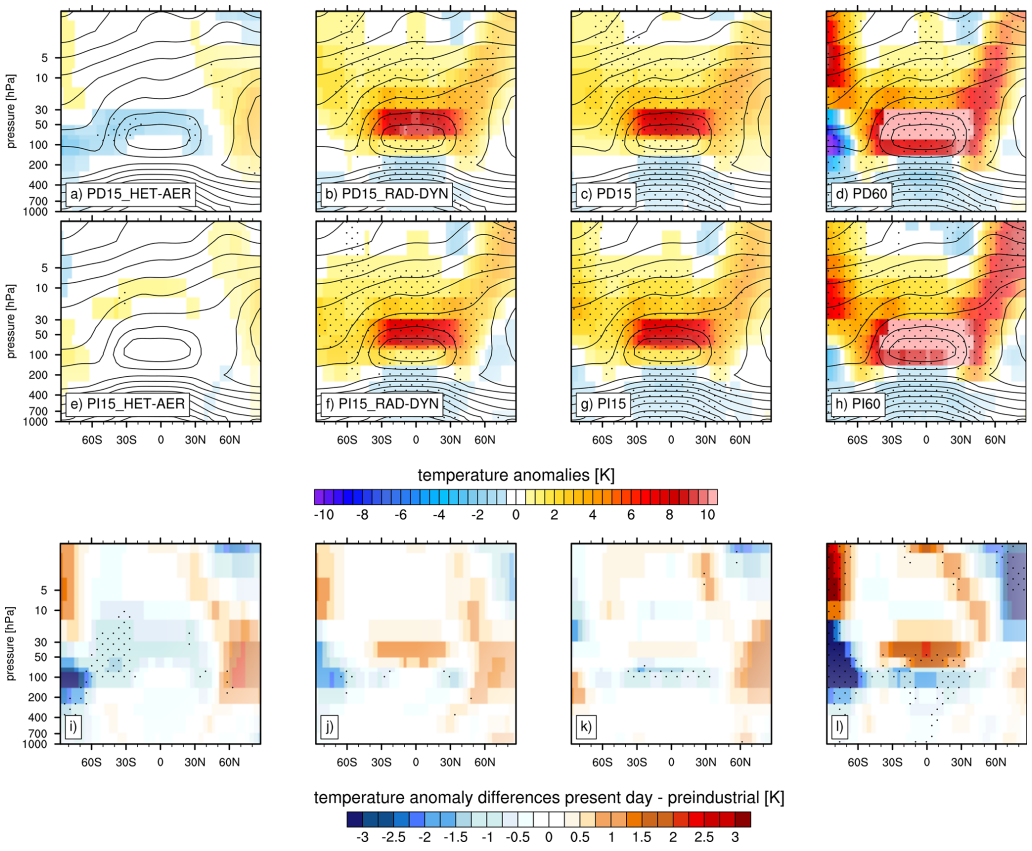

Figure 5. Zonal mean temperature anomalies (K) for the first post eruption winter (DJF) relative to the average of the present-day or preindustrial control simulations: **(a)** anomalies due to the effect of heterogeneous aerosol chemical reactions (HET-AER) for the 15 Tg eruption under present-day conditions, **(b)** same as **(a)**, but for the radiative effects of the aerosols, **(c)** same as **(a)**, but showing the ensemble mean of the full forcing simulations, **(d)** full forcing simulations for the 60 Tg aerosol forcing data set, and **(e–h)** similar to **(a)**, but for preindustrial conditions. Anomalies are calculated relatively to the corresponding control ensemble mean and the stippling in the simulation panels indicates significant differences to the control (Student's t test $p \leq 0.05$). Contours denote the climatological mean DJF temperatures in the control ensembles. **(i–l)** Differences between the present-day and preindustrial temperature anomalies for the different experiments.

anomalies of column ozone cover all latitudes from the subtropics to polar areas (Fig. 3f, compare also S2e, h, l). Consequently, the combined response is dominated by the RAD-DYN effect and the spatial patterns of the anomaly are very similar (Fig. 3g). For larger eruption sizes, the amplitude of the ozone changes due to RAD-DYN effects increases, while heterogeneous chemical reactions on the aerosols are only marginally affected by the eruption strength (Fig. 2).

3.2 Temperature and dynamics

3.2.1 Present-day conditions

One motivation of this study is to ask how the ozone changes described in Sect. 3.1 modulate the dynamical perturbation of the stratosphere due to the volcanic eruption.

Temperature changes associated with an ozone loss due to the HET-AER effect are small compared to the aerosol direct radiative effect, but significant temperature reductions are found in the present-day experiments for all three eruption sizes. For the 15 Tg forcing the cooling reach a minimum of -1 K in the subtropical latitudes of both hemispheres in winter (Fig. 5a). These anomalies increase to more than -2 K for the 60 Tg forcing (not shown). The reduction of the meridional temperature gradient leads to a significant slow-down of the westerly circulation in the polar stratosphere during boreal winter (Fig. 6a) and a weakening of the polar vortex. As index for the NH polar vortex intensity, time series of the zonal mean wind component at 60° N and 10 hPa (Christiansen, 2001, 2005) are shown in Fig. 7. The weakening of this index due to the HET-AER effect is mainly a phenomena of the mid to late winter (January, February). In January the vortex intensity reduces to $35 \pm 15\,\mathrm{m\,s^{-1}}$ in the PD15_HET-AER experiment in comparison to $48 \pm 11\,\mathrm{m\,s^{-1}}$ in the CTRL experiment (32 ± 18 and $36 \pm 11\,\mathrm{m\,s^{-1}}$ for the 30 and 60 Tg experiment, respectively. Compare Fig. 7). During spring a slight (but not significant) vortex intensification is found for the stronger forced ensemble simulations. In March, the mean value of the vortex intensity in CTRL is $9 \pm 18\,\mathrm{m\,s^{-1}}$,

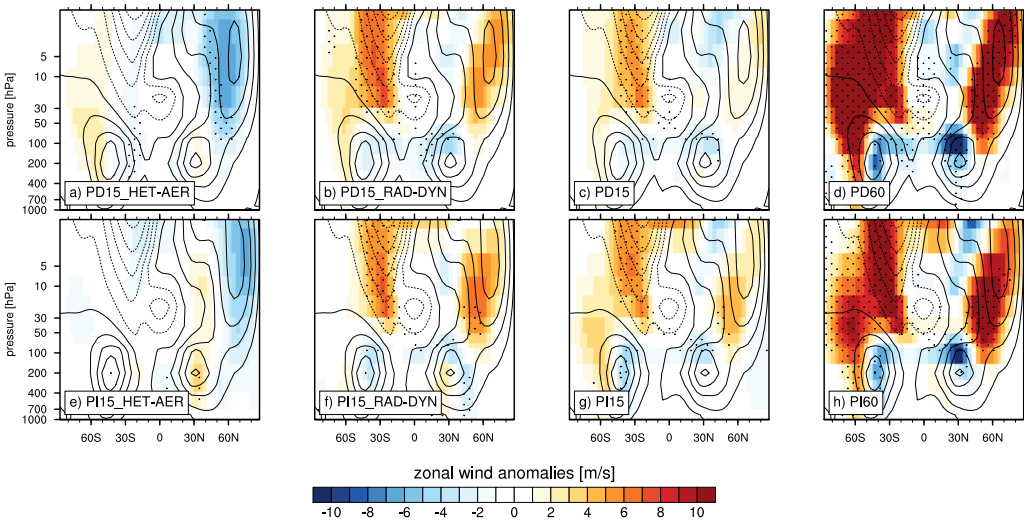

Figure 6. Similar to Fig. 5, but for the zonal mean zonal wind anomalies ($m\,s^{-1}$).

while the vortex in PD15_HET-AER reaches an average of $14\pm15\,m\,s^{-1}$ (21 ± 19 and $19\pm13\,m\,s^{-1}$ for the 30 and 60 Tg experiment, respectively). This spring intensification is probably related to the intensified ozone depletion and associated cooling at polar latitudes. The size of the eruption has no systematic influence on the vortex changes through the HET-AER effect. The HET-AER effect furthermore causes slight positive temperature anomalies in the NH polar stratosphere (Fig. 5a), which are related to the weakening of the polar vortex.

The RAD-DYN effects dominate for the temperature perturbations after the eruption. Significant positive temperature anomalies are found at almost all altitudes and latitudes, with the exception of the polar areas (Fig. 5b). As expected, the temperature anomalies increase with rising aerosol mass. At 50 hPa the maximum temperature anomaly, which occurs around December, is 9.5 K for the 15 Tg and increases to 18.2 and 21.7 K for the 30 and 60 Tg eruptions, respectively. In the troposphere, the expected cooling due to the reduced incoming short-wave flux is found at tropical and subtropical latitudes. The stratospheric warming, however, causes only a weak intensification of the NH polar vortex (Figs. 6b, 7). Significant positive anomalies are found only for a short period in late winter (February, March) in the case of the 15 Tg aerosol forcing. By contrast the ensemble simulations with the 30 and 60 Tg aerosol forcings reveal a significant intensification of the vortex during most of the winter (Fig. 7).

The amplitude of the temperature change through the HET-AER mechanism is much weaker than the changes caused by the RAD-DYN effect (Fig. 5a). Nevertheless, the temperature reduction causes a significant weakening of the NH polar vortex, but only a slight increase in the vortex intensity is found for the RAD-DYN experiment for the 15 Tg aerosol forcing (Fig. 7). The difference in the response of the NH polar vortex is not yet fully understood. It may be related to the different patterns of the temperature anomaly. The aerosol induced warming covers all latitudes up to 60° N in the lower and middle stratosphere and reaches even polar latitudes in the upper stratosphere. By contrast, the cooling associated with the HET-AER effect is limited to the SH and up to 30° N due to the seasonal cycle of the Brewer–Dobson circulation.

3.2.2 Preindustrial conditions

Under preindustrial conditions the response to an eruption differs in several aspects. Similar to the ozone anomalies, the HET-AER effect on the stratospheric temperatures (Fig. 5e, i) and dynamics is very small (Figs. 6e, 7). No significant anomalies are found, not even for the strongest forcing scenario although the tendency of a slight NH polar vortex weakening is apparent, in particular in late winter.

RAD-DYN effects in a present-day atmosphere slightly differ from the response under present-day conditions. At 50 hPa the maximum tropical stratospheric warming is 1.0 K larger in the present-day atmosphere (Fig. 5j) and this differences increases to 2.3 and 1.7 K for the 30 and 60 Tg eruption. The stronger warming under present-day conditions is not related to the dynamical ozone changes in the RAD-DYN ensemble experiment, as will be shown below (Sect. 3.3). A possible explanation could be found in the different background states. Due to the ozone depletion in the present-day atmosphere, stratospheric ozone concentrations are substantially reduced in the present-day tropical lower stratosphere. Furthermore, GHGs are higher for present-day conditions and both differences lead to a colder tropical stratosphere. With a colder stratosphere and a warmer troposphere the radiative heating from below is stronger in the present-day atmosphere. For the combined response in a preindustrial climate setting, no differences to the RAD-DYN results are

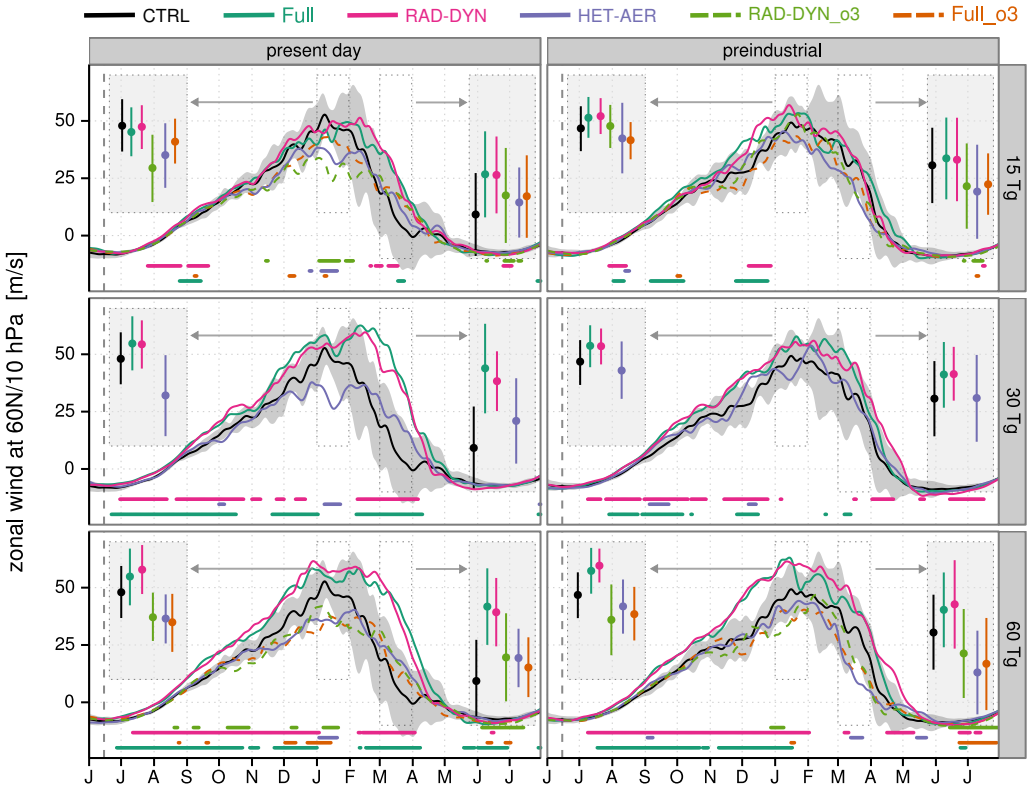

Figure 7. Daily zonal mean zonal wind at 60° N [$m\,s^{-1}$] used as index for the NH polar vortex intensity. Dots at the bottom of each panel indicate days with significant differences to the control ensemble ($p \leq 0.05$). All values are smoothed with an 11 day low pass filter. The start of the eruption (middle of June) is indicated by the vertical dashed line. The shading indicates the standard deviation in the control experiments. Additionally, each panel displays the monthly mean statistics for January (left) and March (right) with the dots representing the mean value and the line range corresponding to the standard deviation for each ensemble experiment.

found, neither for the 15 Tg (Fig. 5g) nor for the stronger forcings.

In terms of the NH polar vortex, the largest differences between preindustrial and present-day conditions are found between the two CTRL experiments (Fig. 7). In January the vortex is slightly stronger in the present-day experiment (PD_CTRL: $48 \pm 11\,m\,s^{-1}$; PI_CTRL: $47 \pm 10\,m\,s^{-1}$), while during March a pronounced and significant weakening of the vortex is obvious for present day (9 ± 18 vs. $31 \pm 16\,m\,s^{-1}$). These differences are also related to the stratospheric temperature differences between preindustrial and present day caused by different GHGs concentrations. Consequently, pronounced differences for the RAD-DYN or full forcing effect would be found between preindustrial and present day, when the vortex response is expressed in terms of anomalies to the corresponding CTRL.

3.3 Effects of the coupling between ozone and stratospheric dynamics on the stratosphere

The simulated ozone changes due to the RAD-DYN effect or in the full forcing response could amplify or weaken the dynamical perturbation of the stratosphere. However, from the results described above, possible feedbacks between the ozone chemistry and the dynamics are difficult to extract. Two additional sensitivity ensemble experiments were therefore performed, driven only by the simulated ensemble mean ozone changes obtained from the RAD-DYN and full forcing experiments (shown for instance in Figs. 2 and 3).

Zonal mean temperature anomalies (Fig. 8) reveal an amplification of the RAD-DYN heating in the lower tropical stratosphere by the ozone chemistry. At these levels, ozone anomalies up to 0.2 ppmv (25 %) are found in the PD15_RAD-DYN ensemble mean, resulting in temperature anomalies of about 1.2 ± 0.3 K (80 hPa) during the first winter season after the eruption (Fig. 8a). Ozone anomalies and temperature anomalies increase with eruption size and reach 0.4 ppmv and 2.9 ± 0.5 K for the 60 Tg eruption the present-day experiments (Fig. 8c). For the ozone changes extracted from the full forcing experiment, the impact on tropical stratospheric temperatures is always weaker, due to the ozone depleting effect of heterogeneous chemical reactions (Fig. 8b, d). Under preindustrial conditions, the response is slightly stronger, but the differences are not significant (Fig. 8e, f, g, h).

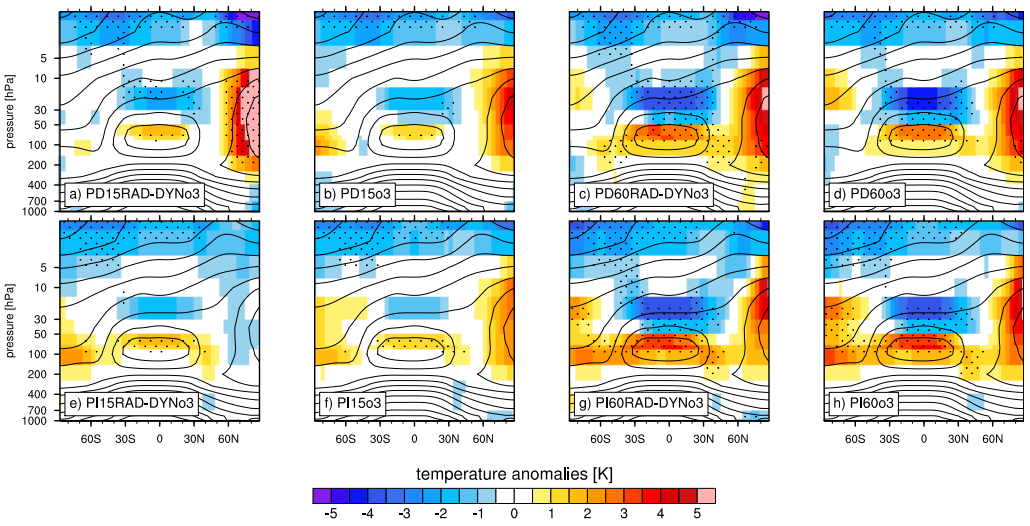

Figure 8. Similar to Fig. 5 but showing DJF zonal mean temperature anomalies (K) in the ozone sensitivity ensemble experiment. (top) Present day ensemble experiments forced by ozone changes from PD15_RAD-DYN **(a)**, PD15 **(b)**, PD60_RAD-DYN **(c)**, and PD60 **(d)**. (bottom) Same forcings but for the preindustrial experiments. Note the different colour scaling in comparison to Fig. 5.

The combined influence of HET-AER and RAD-DYN mechanisms is again visible in the full forcing experiment. The stratospheric warming is slightly reduced by heterogeneous chemical reactions (8.7 K in PD15) and the dynamical changes are weaker in comparison to the RAD-DYN experiment (Fig. 6c). In particular the NH polar vortex weakening in January and the strengthening in March caused by the HET-AER effect is clearly visible in the ū60 index (Fig. 7).

RAD-DYN ozone changes in the tropics furthermore produce a cooling above 30 hPa with temperature anomalies from −2 K (15 Tg) to −4 K (60 Tg). Ozone changes in this region therefore weaken the warming effect of the aerosols. Heterogeneous chemical reactions have no effect on temperatures in this region and ozone changes from the RAD-DYN and the full forcing ensemble simulations lead to very similar temperature patterns. Temperature anomalies in a preindustrial atmosphere do not significantly differ from the results obtained under present day conditions. Note, that the cold anomaly in the upper stratosphere and mesosphere (present in all panels of Fig. 8) can not be attributed to volcanic induced ozone anomalies but is related to the missing diurnal cycle of ozone variations in SOCOL-MPIOM without interactive chemistry (Muthers et al., 2014b).

Furthermore, positive temperature anomalies are found in the NH polar stratosphere, though not significant except for one experiment (ozone changes from PD15_RAD-DYN). Since ozone anomalies in the NH polar stratosphere are very weak during the first winter after an eruption, these warm anomalies are probably not related to the ozone chemistry, but to dynamical changes.

The effect of the ozone perturbations on the NH polar vortex is in general small (Fig. 7) and not always consistent. Nevertheless, all experiments under present-day conditions reveal a slight weakening of the vortex, which is significant for a few days in mid-winter, and a slight (non significant) intensification in late winter. The size of the anomalies is roughly comparable to the changes related to the HET-AER effect. The response of the vortex to the ozone changes from the RAD-AER and full forcing experiment is weaker and not significant when ensemble simulations under preindustrial conditions are considered.

4 Discussion and conclusions

This study addresses the role of ozone changes for the dynamical perturbations of the stratosphere after strong tropical volcanic eruptions. Thereby, the underlying mechanisms and the influence of the climate setting and the eruption strengths are considered. The results are based on a number of ensemble sensitivity simulations with the AOCCM SOCOL-MPIOM, which allows us to separate the effect of heterogeneous chemical reactions from the warming effect of the aerosols for preindustrial and present-day conditions as well as three different eruption intensities.

In agreement with earlier studies we find that both processes, heterogeneous chemical reactions on the aerosol surface and the warming effect of the aerosols are important for the ozone changes after the eruption in an atmosphere with enhanced concentrations of ODS (Pitari and Rizi, 1993; Al-Saadi et al., 2001). A comparable case-study for the 1991 Mt. Pinatubo was performed by Aquila et al. (2013), with a similar separation between radiative-dynamical and heterogeneous chemical effects on the aerosols. They identified a combination of HET-AER and RAD-DYN processes to be responsible for the ozone anomalies in the SH. In particu-

lar they found similar anomalies in the residual mean circulation being responsible for reduced ozone in the tropics and enhanced ozone concentrations at mid-latitudes (compare Fig. 4b and their Fig. 7). This response, however, is limited to the early phase of the eruptions and in combination with the phase of the Brewer–Dobson circulation the anomaly-pattern is found only in the SH. In boreal winter, when tropical stratospheric temperature anomalies are at maximum in our experiments, our findings suggest a similar response of the residual mean circulation in the NH with positive column ozone anomalies at mid-latitudes. Aquila et al. (2013) did not simulate positive column ozone anomalies in the NH related to radiative-dynamical changes (compare their Fig. 6) and concluded that NH ozone anomalies are mainly affected by HET-AER effects. This difference in the response is not yet understood, but may be related to differences in the aerosol forcings. Understanding the response to the RAD-DYN mechanism is of particular importance for volcanic eruptions under preindustrial conditions with low load of ozone depleting halogens, where chemical effects become weak and the response is dominated by radiative-dynamical effects.

The dynamical perturbation of the stratosphere is dominated by the RAD-DYN effect of the aerosols. During winter time, the warming in the tropical stratosphere increases the meridional temperature gradient towards the poles and strengthens the westerly circulation in the polar stratosphere. Ozone changes, related to heterogeneous chemical reactions on aerosols under present-day conditions weaken the warming in the tropical stratosphere and the NH polar vortex. By contrast, ozone changes related to the RAD-DYN mechanism amplify the warming in the subtropical and mid-latitude lower stratosphere, but weaken the temperature response in the middle stratosphere. The latter causes a slight weakening of the polar vortex. In agreement with Stenchikov et al. (2002) and Shindell et al. (2003) we found an intensification of the NH polar vortex in late winter due to ozone changes after strong volcanic eruptions in a present-day atmosphere. Our results show that both, HET-AER and RAD-DYN effects contribute to this intensification.

The atmospheric composition influences the response of the ozone chemistry and the dynamical response to the volcanic aerosols in a significant way. As already shown by Tie and Brasseur (1995) heterogeneous chemical reactions on the aerosol surface cause pronounced global ozone depletion when stratospheric loads of ozone depleting halogens are high, but has only a weak positive effect in a preindustrial atmosphere. Furthermore, ozone depletion scales with the amplitude of eruptions under present-day conditions, but for a preindustrial atmosphere the response is independent from the eruption size (Tie and Brasseur, 1995). With the projected reduction of ODS (Austin and Wilson, 2006; Eyring et al., 2007; Austin et al., 2010) the effect of heterogeneous chemical reactions can be expected to become less important for future eruptions. However, differences in the background state affect the results of this study as well. In recent decades, the stratosphere has undergone a pronounced cooling trend (e.g. Thompson et al., 2012), related to the ozone changes and the increasing levels of GHG (Shine et al., 2003). This cooling also affects the meridional temperature profiles in the stratosphere and the dynamics. In this study, significant differences in the vortex behaviour exist between the control simulations for preindustrial and present day, and these differences can be larger than the differences between the simulations perturbed by the volcanic eruption.

A direct comparison of our results to observations is difficult given the highly idealised character of our experiments. Nevertheless, one experiment, the 15 Tg experiment for the full aerosol effects under present-day conditions, can be considered similar to the perturbation from Pinatubo in 1991. Globally, the combined aerosol effect for the 15 Tg aerosol forcing results in an ozone loss of 10.4 ± 3.7 DU 21 months after the start of the eruption. This agrees reasonably well with observations for Pinatubo (Bodeker et al., 2005), where a reduction of -13.9 DU was observed peaking in May 1993 (22 months after the eruption). Furthermore, the pattern of column ozone anomalies in Bodeker et al. (2005) is similar to the pattern found in the PD15 ensemble mean (Fig. 3). After the eruption, negative anomalies are found in the tropics and positive anomalies in the sub-tropics and mid latitudes. The magnitude of both is stronger in SOCOL-MPIOM than in observations. In particular, the positive column ozone anomaly in the NH mid-latitudes is weaker in the Bodeker et al. (2005) data set. This may be related to the QBO effect (Telford et al., 2009; Randel and Wu, 1995) or the Brewer–Dobson circulation (Aquila et al., 2013), which modulated the ozone anomalies after Pinatubo. The modulating effect of the QBO, however, has been removed by the comparison to an ensemble of control simulations nudged by the same QBO reconstruction. Overestimated ozone anomalies in the PD15 ensemble may further be related to the too strong warming simulated in the tropical stratosphere by SOCOL-MPIOM. The remaining anomalies, i.e. the polar ozone depletion and the global reduction of columns ozone about 1 year after the eruptions agrees reasonable well with the simulated anomalies. For the vertical pattern of ozone changes (e.g. Hassler et al., 2008) the agreement between model results and observations is also reasonable, with the exception of stronger anomalies in the model, in particular in the tropics.

A caveat of this study is the overestimated warming in the tropical stratosphere, which may lead to an overestimation of the dynamical response and the resulting ozone changes. This needs to be considered when interpreting the results of the RAD-DYN and full forcing ensemble results. An overestimation of the lower stratospheric warming after volcanic eruptions is a feature common to many models (e.g. Driscoll et al., 2012). The maximum warming after the Pinatubo eruption in a multi-model ensemble average of 13 CMIP5 models (model selection as in Driscoll et al., 2012) is 3.8 ± 2.9 K for the temperature anomaly at

50 hPa, while reanalysis products and observations suggest temperature anomalies between 2.5 and 3 K (Labitzke and McCormick, 1992; Dee et al., 2011). However, the phase of the QBO and other dynamical processes are suggested to reduce the stratospheric warming after Pinatubo (Driscoll et al., 2012; Fueglistaler et al., 2014). SOCOL-MPIOM simulates a warming of 8.7 ± 1.2 K in the PD15 ensemble. Our results show that the overestimated warming is to some extent related to the ozone changes, which amplify the warming by about 0.9 K (15 Tg forcing at 50 hPa). The aerosol forcing applied in this study also contributes to the overestimated warming. We use a 2-D global aerosol forcing produced by an aerosol micro-physical model, which allows us to generate physical consistent forcing for different eruption intensities. This model-generated forcing differs from satellite based observations for Pinatubo in several aspects (as described by Arfeuille et al., 2013). For comparison, we also perform eight simulations forced by realistic satellite based aerosol concentrations for the Mt. Pinatubo eruption (SAGE_4λ in Arfeuille et al., 2013). In these simulations (not shown) the stratospheric warming is still overestimated (maximum temperature anomalies: 6.0 ± 1.0 K), but the agreement to CMIP5 is better, in particular when the temperature effect of the ozone changes is considered.

In summary, we show that ozone is affected globally by a volcanic eruption for several years. Both effects, the radiative dynamical perturbation by the volcanic aerosols as well as the heterogeneous chemical reaction on the aerosols are important for the response of the ozone chemistry. The climate setting, in particular the atmospheric concentrations of ODS, has the strongest effects on the heterogeneous chemical effect on aerosol surfaces with pronounced global ozone depletion for present-day ODS concentrations (peak reductions of -13, -18, and -21 DU for the 15, 30, and 60 Tg eruptions, respectively) and slight ozone increase for preindustrial ODS concentrations (between 4 and 5 DU for all eruptions). Radiative dynamical ozone changes are positive for preindustrial and present-day conditions, but for present day the response is weakened by amplified polar ozone depletion ($+5$, $+8$, $+12$ DU peak column ozone anomalies for present day and $+6$, $+14$, $+18$ DU for preindustrial). The full effect of the volcanic aerosol, therefore, clearly differs between preindustrial and present day, with long lasting ozone depletion in a present-day atmosphere and positive ozone anomalies for preindustrial conditions. The response of stratospheric temperature and dynamics is dominated by the radiative heating effect of the aerosols. A small influence of the climate setting on the heating of the lower tropical stratosphere was found, with larger temperature anomalies for the present-day experiments. Dynamical radiative ozone changes further amplify the stratospheric temperature anomalies in the lower tropical stratosphere (and cause a cooling in higher levels). Ozone changes due to heterogeneous chemical reactions on the aerosols are responsible for a slight cooling of the tropical stratosphere. In winter and early spring after the eruption, the NH polar vortex is intensified, due to the radiative warming in the tropical stratosphere. Ozone changes, either due to radiative-dynamical effects or heterogeneous reaction on the aerosol surface, induce a slight weakening of the vortex in mid-winter. In late winter they cause a slight strengthening of the westerly circulation in the NH polar stratosphere.

The Supplement related to this article is available online at doi:10.5194/acp-15-11461-2015-supplement.

Acknowledgements. We would like to thank the two anonymous reviewers for their constructive comments. This work has been supported by the Swiss National Science Foundation under grant CRSII2-147659 (FUPSOL II) and profited from discussions during the PAGES/FUPSOL Workshop in 2014.

Edited by: K. Tsigaridis

References

Al-Saadi, J. A., Pierce, R. B., Fairlie, T. D., Kleb, K. M., Eckman, R. S., Grose, W. L., Natarajan, M., and Olson, J. R.: Response of middle atmosphere chemistry and dynamics to volcanically elevated sulfate aerosol: three-dimensional coupled model simulations, J. Geophys. Res., 106, 27255–27275, doi:10.1029/2000JD000185, 2001.

Andrews, D. G., Holton, J. R., and Leovy, C. B.: Middle Atmosphere Dynamics, Academic Press, Orlando, USA, 1987.

Anet, J. G., Muthers, S., Rozanov, E., Raible, C. C., Peter, T., Stenke, A., Shapiro, A. I., Beer, J., Steinhilber, F., Brönnimann, S., Arfeuille, F., Brugnara, Y., and Schmutz, W.: Forcing of stratospheric chemistry and dynamics during the Dalton Minimum, Atmos. Chem. Phys., 13, 10951–10967, doi:10.5194/acp-13-10951-2013, 2013.

Aquila, V., Oman, L. D., Stolarski, R., Douglass, A. R., and Newman, P. A.: The response of ozone and nitrogen dioxide to the eruption of Mt. Pinatubo at southern and northern midlatitudes, J. Atmos. Sci., 70, 894–900, doi:10.1175/JAS-D-12-0143.1, 2013.

Arfeuille, F., Luo, B. P., Heckendorn, P., Weisenstein, D., Sheng, J. X., Rozanov, E., Schraner, M., Brönnimann, S., Thomason, L. W., and Peter, T.: Modeling the stratospheric warming following the Mt. Pinatubo eruption: uncertainties in aerosol extinctions, Atmos. Chem. Phys., 13, 11221–11234, doi:10.5194/acp-13-11221-2013, 2013.

Arfeuille, F., Weisenstein, D., Mack, H., Rozanov, E., Peter, T., and Brönnimann, S.: Volcanic forcing for climate modeling: a new microphysics-based data set covering years 1600–present, Clim. Past, 10, 359–375, doi:10.5194/cp-10-359-2014, 2014.

Austin, J. and Wilson, R. J.: Ensemble simulations of the decline and recovery of stratospheric ozone, J. Geophys. Res., 111, D16314, doi:10.1029/2005JD006907, 2006.

Austin, J., Scinocca, J., Plummer, D., Oman, L., Waugh, D., Akiyoshi, H., Bekki, S., Braesicke, P., Butchart, N., Chipperfield,

M., Cugnet, D., Dameris, M., Dhomse, S., Eyring, V., Frith, S., Garcia, R. R., Garny, H., Gettelman, A., Hardiman, S. C., Kinnison, D., Lamarque, J. F., Mancini, E., Marchand, M., Michou, M., Morgenstern, O., Nakamura, T., Pawson, S., Pitari, G., Pyle, J., Rozanov, E., Shepherd, T. G., Shibata, K., Teyssèdre, H., Wilson, R. J., and Yamashita, Y.: Decline and recovery of total column ozone using a multimodel time series analysis, J. Geophys. Res., 115, D00M10, doi:10.1029/2010JD013857, 2010.

Austin, J., Horowitz, L. W., Schwarzkopf, M. D., Wilson, R. J., and Levy, H.: Stratospheric ozone and temperature simulated from the preindustrial era to the present day, J. Climate, 26, 3528–3543, doi:10.1175/JCLI-D-12-00162.1, 2013.

Bodeker, G. E., Shiona, H., and Eskes, H.: Indicators of Antarctic ozone depletion, Atmos. Chem. Phys., 5, 2603–2615, doi:10.5194/acp-5-2603-2005, 2005.

Brasseur, G. and Granier, C.: Mount Pinatubo aerosols, chlorofluorocarbons, and ozone depletion, Science, 257, 1239–42, doi:10.1126/science.257.5074.1239, 1992.

Budich, R., Gioretta, M., Jungclaus, J., Redler, R., and Reick, C.: The MPI-M Millennium Earth System Model: an assembling guide for the COSMOS configuration, MPI report, Max-Planck Institute for Meteorology, Hamburg, Germany, 2010.

Carslaw, K. S., Luo, B. P., Clegg, S. L., Peter, T., Brimblecombe, P., and Crutzen, P. J.: Stratospheric aerosol growth and HNO_3 gas phase depletion from coupled HNO_3 and water uptake by liquid particles, Geophys. Res. Lett., 21, 2479–2482, doi:10.1029/94GL02799, 1994.

Carslaw, K. S., Luo, B., and Peter, T.: An analytic expression for the composition of aqueous aerosols including gas phase removal of $HNO_3-H_2SO_4$ stratospheric aerosols including gas phase removal of HNO_3, Geophys. Res. Lett., 22, 1877–1880, 1995.

Christiansen, B.: Downward propagation of zonal mean zonal wind anomalies from the stratosphere to the troposphere: model and reanalysis, J. Geophys. Res., 106, 27307, doi:10.1029/2000JD000214, 2001.

Christiansen, B.: Downward propagation and statistical forecast of the near-surface weather, J. Geophys. Res., 110, D14104, doi:10.1029/2004JD005431, 2005.

Christiansen, B.: Volcanic eruptions, large-scale modes in the Northern Hemisphere, and the El Niño-Southern Oscillation, J. Climate, 21, 910–922, doi:10.1175/2007JCLI1657.1, 2008.

Cole-Dai, J.: Volcanoes and climate, Wiley Interdisciplinary Reviews: Climate Change, 1, 824–839, doi:10.1002/wcc.76, 2010.

Dee, D. P., Uppala, S. M., Simmons, A. J., Berrisford, P., Poli, P., Kobayashi, S., Andrae, U., Balmaseda, M. A., Balsamo, G., Bauer, P., Bechtold, P., Beljaars, A. C. M., van de Berg, L., Bidlot, J., Bormann, N., Delsol, C., Dragani, R., Fuentes, M., Geer, A. J., Haimberger, L., Healy, S. B., Hersbach, H., Hólm, E. V., Isaksen, L., Kållberg, P., Köhler, M., Matricardi, M., McNally, A. P., Monge-Sanz, B. M., Morcrette, J.-J., Park, B.-K., Peubey, C., de Rosnay, P., Tavolato, C., Thépaut, J.-N., and Vitart, F.: The ERA-Interim reanalysis: configuration and performance of the data assimilation system, Q. J. Roy. Meteor. Soc., 137, 553–597, doi:10.1002/qj.828, 2011.

Dhomse, S. S., Emmerson, K. M., Mann, G. W., Bellouin, N., Carslaw, K. S., Chipperfield, M. P., Hommel, R., Abraham, N. L., Telford, P., Braesicke, P., Dalvi, M., Johnson, C. E., O'Connor, F., Morgenstern, O., Pyle, J. A., Deshler, T., Zawodny, J. M., and Thomason, L. W.: Aerosol microphysics simulations of the Mt. Pinatubo eruption with the UM-UKCA composition-climate model, Atmos. Chem. Phys., 14, 11221–11246, doi:10.5194/acp-14-11221-2014, 2014.

Driscoll, S., Bozzo, A., Gray, L. J., Robock, A., and Stenchikov, G.: Coupled Model Intercomparison Project 5 (CMIP5) simulations of climate following volcanic eruptions, J. Geophys. Res., 117, D17105, doi:10.1029/2012JD017607, 2012.

Egorova, T., Rozanov, E., Zubov, V., and Karol, I. L.: Model for Investigating Ozone Trends (MEZON), Izv. Atmos. Ocean. Phys.+, 39, 277–292, 2003.

Egorova, T., Rozanov, E., Manzini, E., Schmutz, W., and Peter, T.: Chemical and dynamical response to the 11-year variability of the solar irradiance simulated with a chemistry–climate model, Geophys. Res. Lett., 83, 6225–6230, 2004.

Eyring, V., Waugh, D. W., Bodeker, G. E., Cordero, E., Akiyoshi, H., Austin, J., Beagley, S. R., Boville, B. A., Braesicke, P., Brühl, C., Butchart, N., Chipperfield, M. P., Dameris, M., Deckert, R., Deushi, M., Frith, S. M., Garcia, R. R., Gettelman, A., Giorgetta, M. A., Kinnison, D. E., Mancini, E., Manzini, E., Marsh, D. R., Matthes, S., Nagashima, T., Newman, P. A., Nielsen, J. E., Pawson, S., Pitari, G., Plummer, D. A., Rozanov, E., Schraner, M., Scinocca, J. F., Semeniuk, K., Shepherd, T. G., Shibata, K., Steil, B., Stolarski, R. S., Tian, W., and Yoshiki, M.: Multimodel projections of stratospheric ozone in the 21st century, J. Geophys. Res., 112, D16303, doi:10.1029/2006JD008332, 2007.

Fischer, E. M., Luterbacher, J., Zorita, E., Tett, S. F. B., Casty, C., and Wanner, H.: European climate response to tropical volcanic eruptions over the last half millennium, Geophys. Res. Lett., 34, 1–6, doi:10.1029/2006GL027992, 2007.

Fleming, E. L., Jackman, H., Stolarski, S., and Considine, D. B.: Simulation of stratospheric tracers using an improved empirically based two-dimensional model transport formulation and equatorial, J. Geophys. Res., 104, 23911–23934, doi:10.1029/1999JD900332, 1999.

Forster, P., Ramaswamy, V., Artaxo, P., Berntsen, T., Betts, R., Fahey, D. W., Haywood, J., Lean, J., Lowe, D. C., Myhre, G., Nganga, J., Prinn, R., Raga, G., Schulz, M., and Van Dorland, R.: Changes in Atmospheric Constituents and in Radiative Forcing, chap. 2, Cambridge University Press, Cambridge, United Kingdom, New York, 2007.

Fueglistaler, S., Abalos, M., Flannaghan, T. J., Lin, P., and Randel, W. J.: Variability and trends in dynamical forcing of tropical lower stratospheric temperatures, Atmos. Chem. Phys., 14, 13439–13453, doi:10.5194/acp-14-13439-2014, 2014.

Gao, C., Robock, A., and Ammann, C.: Volcanic forcing of climate over the past 1500 years: an improved ice core-based index for climate models, J. Geophys. Res., 113, D23111, doi:10.1029/2008JD010239, 2008.

Giorgetta, M. A., Bengtsson, L., and Arpe, K.: An investigation of QBO signals in the east Asian and Indian monsoon in GCM experiments, Clim. Dynam., 15, 435–450, doi:10.1007/s003820050292, 1999.

Graf, H.-F., Kirchner, I., Robock, A., and Schult, I.: Pinatubo eruption winter climate effects: model versus observations, Clim. Dynam., 92, 81–93, 1993.

Grainger, R. G., Lambert, A., Rodgers, C. D., Taylor, F. W., and Deshler, T.: Stratospheric aerosol effective radius, surface area and volume estimated from infrared measurements, J. Geophys. Res., 100, 16507, doi:10.1029/95JD00988, 1995.

Grant, W. B., Browell, E. V., Fishman, J., Brackett, V. G., Veiga, R. E., Nganga, D., Minga, A., Cros, B., Butler, C. F., Fenn, M. A., Long, C. S., and Stowe, L. L.: Aerosol-associated changes in tropical stratospheric ozone following the eruption of Mount Pinatubo, J. Geophys. Res., 99, 8197, doi:10.1029/93JD03314, 1994.

Guo, S., Rose, W. I., Bluth, G. J. S., and Watson, I. M.: Particles in the great Pinatubo volcanic cloud of June 1991: the role of ice, Geochem. Geophy. Geosy., 5, 1–35, doi:10.1029/2003GC000655, 2004.

Hassler, B., Bodeker, G. E., and Dameris, M.: Technical Note: A new global database of trace gases and aerosols from multiple sources of high vertical resolution measurements, Atmos. Chem. Phys., 8, 5403–5421, doi:10.5194/acp-8-5403-2008, 2008.

Heckendorn, P., Weisenstein, D., Fueglistaler, S., Luo, B. P., Rozanov, E., Schraner, M., Thomason, L. W., and Peter, T.: The impact of geoengineering aerosols on stratospheric temperature and ozone, Environ. Res. Lett., 4, 045108, doi:10.1088/1748-9326/4/4/045108, 2009.

Jungclaus, J. H., Keenlyside, N., Botzet, M., Haak, H., Luo, J.-J., Latif, M., Marotzke, J., Mikolajewicz, U., and Roeckner, E.: Ocean circulation and tropical variability in the coupled model ECHAM5/MPI-OM, J. Climate, 19, 3952–3972, doi:10.1175/JCLI3827.1, 2006.

Kodera, K.: Influence of volcanic eruptions on the troposphere through stratospheric dynamical processes in the Northern Hemisphere winter, J. Geophys. Res., 99, 1273–1282, 1994.

Labitzke, K. and McCormick, M. P.: Stratospheric temperature increases due to Pinatubo aerosols, Geophys. Res. Lett., 19, 207–210, 1992.

Manzini, E., Giorgetta, M. A., Esch, M., Kornblueh, L., and Roeckner, E.: The influence of sea surface temperatures on the northern winter stratosphere: ensemble simulations with the MAECHAM5 model, J. Climate, 19, 3863–3881, doi:10.1175/JCLI3826.1, 2006.

Marsland, S.: The Max-Planck-Institute global ocean/sea ice model with orthogonal curvilinear coordinates, Ocean Model., 5, 91–127, doi:10.1016/S1463-5003(02)00015-X, 2003.

Muthers, S., Anet, J. G., Raible, C. C., Brönnimann, S., Rozanov, E., Arfeuille, F., Peter, T., Shapiro, A. I., Beer, J., Steinhilber, F., Brugnara, Y., and Schmutz, W.: Northern hemispheric winter warming pattern after tropical volcanic eruptions: sensitivity to the ozone climatology, J. Geophys. Res., 110, 1340–1355, doi:10.1002/2013JD020138, 2014a.

Muthers, S., Anet, J. G., Stenke, A., Raible, C. C., Rozanov, E., Brönnimann, S., Peter, T., Arfeuille, F. X., Shapiro, A. I., Beer, J., Steinhilber, F., Brugnara, Y., and Schmutz, W.: The coupled atmosphere–chemistry–ocean model SOCOL-MPIOM, Geosci. Model Dev., 7, 2157–2179, doi:10.5194/gmd-7-2157-2014, 2014b.

Pitari, G. and Rizi, V.: An estimate of the chemical and radiative perturbation of stratospheric ozone following the eruption of Mt. Pinatubo, J. Atmos. Sci., 50, 3260–3276, 1993.

Pitari, G., Aquila, V., Kravitz, B., Robock, A., Watanabe, S., Cionni, I., De Luca, N., Di Genova, G., Mancini, E., and Tilmes, S.: Stratospheric ozone response to sulfate geoengineering: results from the Geoengineering Model Intercomparison Project (GeoMIP), J. Geophys. Res., 119, 2629–2653, doi:10.1002/2013JD020566, 2014.

Portmann, R. W., Solomon, S., Garcia, R. R., Thomason, L. W., Poole, L. R., and Mccormick, M. P.: Role of aerosol variations in anthropogenic ozone depletion in the polar regions paper, J. Geophys. Res., 101, 22991–23006, doi:10.1029/96JD02608, 1996.

Randel, W. J., Wu, F., Russel, J. M., Waters, J. W., and Froidevaux, L.: Ozone and temperature changes in the stratosphere following the eruption of Mount Pinatubo, J. Geophys. Res., 100, 16753–16764, doi:10.1029/95JD01001, 1995.

Robock, A.: Volcanic eruptions and climate, Rev. Geophys., 38, 191–219, 2000.

Robock, A. and Mao, J.: Winter warming from large volcanic eruptions, Geophys. Res. Lett., 12, 2405–2408, 1992.

Roeckner, E., Bäuml, G., Bonaventura, L., Brokopf, R., Esch, M., Giorgetta, M., Hagemann, S., Kirchner, I., Kornblueh, L., Manzini, E., Rhodin, A., Schlese, U., Schulzweida, U., and Tompkins, A.: The atmospheric general circulation model ECHAM5 – model description, MPI report 349, Max-Planck Institute for Meteorology, Hamburg, Germany, 2003.

Rosenfield, J. E., Considine, D. C., Meade, P. E., Bacmeister, J. T., Jackman, C. H., and Schoeberl, M. R.: Stratospheric effects of Mount Pinatubo aerosol studied with a coupled two-dimensional model, J. Geophys. Res., 102, 3649–3670, doi:10.1029/96JD03820, 1997.

Rozanov, E. V., Schlesinger, M. E., Zubov, V., Yang, F., and Andronova, N. G.: The UIUC three-dimensional stratospheric chemical transport model: description and evaluation of the simulated source gases and ozone, J. Geophys. Res., 104, 11755–11781, doi:10.1029/1999JD900138, 1999.

Rozanov, E. V., Schlesinger, M. E., Andronova, N. G., Yang, F., Malyshev, S. L., Zubov, V. A., Egorova, T. A., and Li, B.: Climate/chemistry effects of the Pinatubo volcanic eruption simulated by the UIUC stratosphere/troposphere GCM with interactive photochemistry, J. Geophys. Res., 107, 4594, doi:10.1029/2001JD000974, 2002.

Schraner, M., Rozanov, E., Schnadt Poberaj, C., Kenzelmann, P., Fischer, A. M., Zubov, V., Luo, B. P., Hoyle, C. R., Egorova, T., Fueglistaler, S., Brönnimann, S., Schmutz, W., and Peter, T.: Technical Note: Chemistry-climate model SOCOL: version 2.0 with improved transport and chemistry/microphysics schemes, Atmos. Chem. Phys., 8, 5957–5974, doi:10.5194/acp-8-5957-2008, 2008.

Shindell, D. T., Schmidt, G. A., Miller, R. L., and Mann, M. E.: Volcanic and solar forcing of climate change during the preindustrial era, J. Climate, 16, 4094–4107, doi:10.1175/1520-0442(2003)016<4094:VASFOC>2.0.CO;2, 2003.

Shindell, D. T., Schmidt, G. A., Mann, M. E., and Faluvegi, G.: Dynamic winter climate response to large tropical volcanic eruptions since 1600, J. Geophys. Res., 109, D05104, doi:10.1029/2003JD004151, 2004.

Shine, K. P., Bourqui, M. S., Forster, P. M. D. F., Hare, S. H. E., Langematz, U., Braesicke, P., Grewe, V., Ponater, M., Schnadt, C., Smith, C. A., Haigh, J. D., Austin, J., Butchart, N., Shindell, D. T., Randel, W. J., Nagashima, T., Portmann, R. W., Solomon, S., Seidel, D. J., Lanzante, J., Klein, S., Ramaswamy, V., and Schwarzkopf, M. D.: A comparison of model-simulated trends in stratospheric temperatures, Q. J. Roy. Meteor. Soc., 129, 1565–1588, doi:10.1256/qj.02.186, 2003.

Solomon, S.: Stratospheric ozone depletion: a review of concepts and history, Rev. Geophys., 37, 275, doi:10.1029/1999RG900008, 1999.

Solomon, S., Portmann, R. W., Garcia, R. R., Thomason, L. W., Poole, L. R., Mccormick, M. P., and Cly, C.: The role of aerosol variations in anthropogenic ozone depletion at northern midlatitudes, J. Geophys. Res., 101, 6713–6727, 1996.

SPARC Report on Lifetimes of Stratospheric Ozone-Depleting Substances, Their Replacements, and Related Species, Tech. rep., SPARC, available at: http://www.sparc-climate.org/publications/sparc-reports/, last access: 8 October 2015, 2013.

Stenchikov, G., Robock, A., Ramaswamy, V., Schwarzkopf, M. D., Hamilton, K., and Ramachandran, S.: Arctic Oscillation response to the 1991 Mount Pinatubo eruption: effects of volcanic aerosols and ozone depletion, J. Geophys. Res., 107, 1–16, doi:10.1029/2002JD002090, 2002.

Stenke, A., Schraner, M., Rozanov, E., Egorova, T., Luo, B., and Peter, T.: The SOCOL version 3.0 chemistry–climate model: description, evaluation, and implications from an advanced transport algorithm, Geosci. Model Dev., 6, 1407–1427, doi:10.5194/gmd-6-1407-2013, 2013.

Telford, P., Braesicke, P., Morgenstern, O., and Pyle, J.: Reassessment of causes of ozone column variability following the eruption of Mount Pinatubo using a nudged CCM, Atmos. Chem. Phys., 9, 4251–4260, doi:10.5194/acp-9-4251-2009, 2009.

Textor, C., Graf, H.-F., Timmreck, C., and Robock, A.: Emissions from volcanoes, in: Emissions of atmospheric trace compounds, Springer, 269–303, 2004.

Thompson, D. W. J., Seidel, D. J., Randel, W. J., Zou, C.-Z., Butler, A. H., Mears, C., Osso, A., Long, C., and Lin, R.: The mystery of recent stratospheric temperature trends, Nature, 491, 692–697 2012.

Tie, X. and Brasseur, G.: The response of stratospheric ozone to volcanic eruptions: sensitivity to atmospheric chlorine loading, Geophys. Res. Lett., 22, 3035–3038, 1995.

Timmreck, C.: Modeling the climatic effects of large explosive volcanic eruptions, Wiley Interdisciplinary Reviews: Climate Change, 3, 545–564, doi:10.1002/wcc.192, 2012.

Timmreck, C., Graf, H.-F., Lorenz, S. J., Niemeier, U., Zanchettin, D., Matei, D., Jungclaus, J. H., and Crowley, T. J.: Aerosol size confines climate response to volcanic super-eruptions, Geophys. Res. Lett., 37, 1–5, doi:10.1029/2010GL045464, 2010.

Valcke, S.: The OASIS3 coupler: a European climate modelling community software, Geosci. Model Dev., 6, 373–388, doi:10.5194/gmd-6-373-2013, 2013.

Weisenstein, D. K., Yue, G. K., Ko, M. K. W., Sze, N. D., Rodriguez, J. M., and Scott, C. J.: A two-dimensional model of sulfur species and aerosols, J. Geophys. Res., 102, 13019–13035, 1997.

Weisenstein, D. K., Penner, J. E., Herzog, M., and Liu, X.: Global 2-D intercomparison of sectional and modal aerosol modules, Atmos. Chem. Phys., 7, 2339–2355, doi:10.5194/acp-7-2339-2007, 2007.

Zanchettin, D., Timmreck, C., Bothe, O., Lorenz, S. J., Hegerl, G., Graf, H.-F., Luterbacher, J., and Jungclaus, J. H.: Delayed winter warming: a robust decadal response to strong tropical volcanic eruptions?, Geophys. Res. Lett., 40, 204–209, doi:10.1029/2012GL054403, 2012.